Editors' Suggestion

Observation of a Dissipative Time Crystal

Hans Keßler,[1,*] Phatthamon Kongkhambut,[1] Christoph Georges,[1] Ludwig Mathey,[1,2] Jayson G. Cosme,[3] and Andreas Hemmerich[1,2]

[1]Zentrum für Optische Quantentechnologien and Institut für Laser-Physik, Universität Hamburg, 22761 Hamburg, Germany
[2]The Hamburg Center for Ultrafast Imaging, Luruper Chaussee 149, 22761 Hamburg, Germany
[3]National Institute of Physics, University of the Philippines, Diliman, Quezon City 1101, Philippines

(Received 21 January 2021; revised 12 April 2021; accepted 28 May 2021; published 19 July 2021)

We present the first experimental realization of a time crystal stabilized by dissipation. The central signature in our implementation in a driven open atom-cavity system is a period doubled switching between distinct checkerboard density wave patterns, induced by the interplay between controlled cavity dissipation, cavity-mediated interactions, and external driving. We demonstrate the robustness of this dynamical phase against system parameter changes and temporal perturbations of the driving.

DOI: 10.1103/PhysRevLett.127.043602

Phase transitions of matter can be associated with the spontaneous breaking of a symmetry. For crystallization, this broken symmetry is the spatial translation symmetry, as the atoms spontaneously localize in a periodic arrangement. In analogy to spatial crystals, the spontaneous breaking of temporal translation symmetry can result in the formation of time crystals. Following its initial proposal [1,2], the possibility of time crystals in the ground state of equilibrium many-body systems was ruled out for fundamental reasons [3,4]. This development led to a paradigm shift, directing the search for time crystals towards genuine nonequilibrium scenarios [5–11]. In particular, the no-go theorem [3,4] can be circumvented by periodic driving, which imposes a discrete time translation symmetry on the system. Floquet or discrete time crystals emerge, when discrete time translation symmetry is spontaneously broken, which manifests as a subharmonic response of an observable [12–15]. Previous experimental studies have focused on driven closed quantum systems with long-lived time crystalline response enabled by many-body mechanisms, which impede excessive heating [5–7,16,17]. However, as proposed by theoretical work [18–22], dissipation and fluctuations, induced via controlled coupling to a suitable environment can also serve as a source for stabilization of time-crystal dynamics.

Here, we report the experimental realization of a dissipative time crystal (DTC) phase in an atom-cavity platform [23]. This is inspired by a recent theoretical proposal for a time crystal stabilized through an interplay between interaction and dissipation in the open Dicke model, arising when the light-matter coupling is periodically modulated [18–20]. The defining feature of this paradigmatic DTC is a subharmonic response, where the system periodically switches between pairs of $\mathbb{Z}_2$ symmetry broken superradiant states.

A Bose-Einstein condensate (BEC) of ^{87}Rb atoms is prepared inside a high-finesse optical cavity pumped by a retroreflected laser beam at wavelength $\lambda_P = 803$ nm, aligned perpendicular to the cavity axis, as depicted in Fig. 1(a). The atom-cavity system operates in the recoil-resolved regime, where the cavity field and the atomic distribution evolve at a similar timescale leading to a retarded infinite-range cavity-mediated interaction between the atoms [24]. Above a critical value of the pump strength ϵ, the system undergoes a self-organization transition from a BEC phase to a density wave (DW) phase, which emulates the superradiant phase transition in the open Dicke model [25,26]. In a spontaneous $\mathbb{Z}_2$ symmetry breaking process, an intracavity optical lattice arises, which traps the atoms either in the black or the white squares of a checkerboard pattern, denoted as odd and even DW.

An effective driving of the light-matter coupling can be realized by modulating the pump strength. Off-resonant driving of the pump strength at a frequency ω_D notably exceeding the recoil frequency $\omega_{\mathrm{rec}} \equiv \hbar k^2/(2m) = 2\pi \times 3.55$ kHz, with $k \equiv 2\pi/\lambda_P$ and the atomic mass m, leads to a dynamical renormalization of the phase boundary between the BEC and DW phases [27,28]. On the other hand, a period doubling response characterized by periodic switching between the odd and even DWs has been predicted for modulating only slightly above the recoil frequency [18,29,30]. This phase, originally addressed as dynamical normal phase [18], shows subharmonic oscillations between the two $\mathbb{Z}_2$ symmetry broken even and odd DW states and is closely related to the DTC phase proposed in the open Dicke model [19]. In the thermodynamic limit, $N \to \infty$, the Dicke model can be transformed into a parametrically driven coupled oscillator system with two polaritonic states. Driving at twice the lower polariton frequency leads to an instability, which gives rise to a period-doubling response in the full atom-cavity model

(cf. Ref. [31]). In the following, we describe the experimental realization of a DTC in our atom-cavity system and analyze its properties as a time crystal.

Each experimental sequence begins with preparing the atom-cavity system in the self-organized DW phase (see Ref. [31]). An example of a time sequence for the pump is shown in Fig. 1(b). For $t < -5T_D$ the system is in the BEC phase. The intracavity photon number N_P is zero and the observed momentum spectrum in the upper panel of Fig. 1(d) shows the BEC mode at zero momentum and two Bragg resonances at $\pm 2\hbar k$ along the y direction, associated with the matter grating induced by the pump wave. This grating is illustrated in the lower panel of Fig. 1(d) by showing the single-particle density distribution obtained from a mean-field model (see Ref. [31]). The self-organization transition into the DW phase is observed in Fig. 1(c) around $t \approx -5T_D$, as evidenced from a significant increase in the intracavity photon number N_P and the locking of the relative phase ϕ between the pump and cavity fields at a constant value $\phi \approx 0$. A momentum spectrum, characteristic for the DW phase, is shown in the upper panel of Fig. 1(e) for $t = 0$. The occupation of the momentum modes $\{p_y, p_z\} = \{\pm\hbar k, \pm\hbar k\}$ signals the formation of an intracavity checkerboard matter grating, as illustrated by the calculated single-particle density distribution, shown in the lower panel. The two possible energetically degenerate DW states can be distinguished by their associated values of the phase $\phi = 0$ or $\phi = \pi$ for odd and even realizations, respectively [37]. We measure N_P and ϕ using a balanced heterodyne detection scheme [38]. The probability for the occurrence of the odd and even DW configurations is found to be close to 50% (see Ref. [31]), which confirms that the discrete symmetry breaking in the chequerboard DW phase is well established in our system.

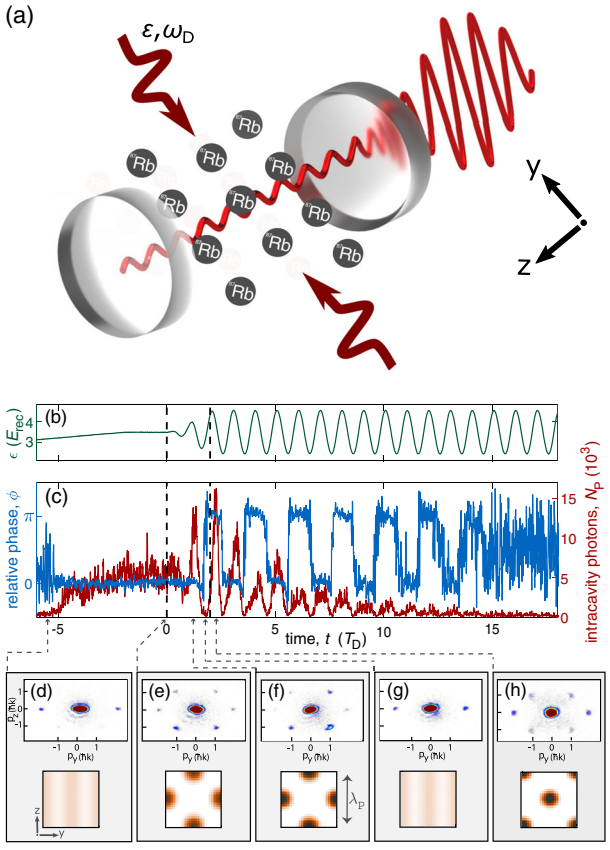

FIG. 1. Dissipative time crystal. (a) Schematic diagram of the transversely pumped atom-cavity system. (b) Time sequence for the pump with modulation strength $f_0 = 0.3$ and modulation period $T_D = 0.25$ ms. In the time interval delimited by dashed lines, f_0 is linearly ramped from zero to its desired value. (c) The corresponding response of the intracavity photon number N_P (red) and the relative phase ϕ between the pump and the cavity light field (blue). (d)–(h) Top panels: momentum distributions measured at instances of time marked by dashed arrows in (c). Bottom panels: corresponding mean-field results for the single-particle density distribution, which shows periodic switching between even and odd DWs at twice the driving period.

Upon preparation of the DW phase, in the time interval delimited by the vertical dashed lines, we linearly increase the modulation strength f_0 in 500 μs from zero to its final value [see Fig. 1(b)]. Subsequently, f_0 is kept constant for 5 ms, such that the pump strength evolves according to $\epsilon = \epsilon_0[1 + f_0 \sin(\omega_D t)]$. The dynamical response seen in Fig. 1(c) for positive t presents the key observation of this work: the emergence of a DTC phase characterized by pulsating behavior of the intracavity photon number N_P (red trace) and a period-doubling response of the relative phase ϕ (blue trace). The presence of intracavity photons highlights the many-body aspect of the DTC phase since they induce a retarded infinite-range interaction or all-to-all coupling between the atoms. The period-doubling dynamics arises in the relative phase ϕ. As ϕ switches from zero to π or vice versa after one modulation cycle, the atomic ensemble self-organizes from one type of checkerboard lattice [see Fig. 1(f)] to its symmetry-broken partner [see Fig. 1(h)]. That is, the system requires two modulation cycles to return to its initial configuration. After half of a modulation period, the system crosses from the DW phase with significant occupation of the cavity mode, to the BEC phase, where the cavity is almost empty. This behavior, corroborated by the momentum distribution in Fig. 1(g), is responsible for the pulsating intracavity photon number in Fig. 1(c) (red trace).

In Figs. 2(a)–(f), we present the various dynamical regimes accessed by tuning the modulation strength. For weak modulation [see Figs. 2(a) and 2(d)], the system stays in the DW phase and the relative phase remains locked to its value before the pump modulation. For intermediate modulation strength, the relative phase exhibits period-doubling dynamics [see Fig. 2(b)], resulting in a subharmonic peak at $\omega = \omega_D/2$ in the Fourier spectrum in Fig. 2(e). Increasing the modulation strength even further leads to chaotic dynamics dominated by heating and loss of spatiotemporal coherence [see Figs. 2(c) and 2(f)]. In

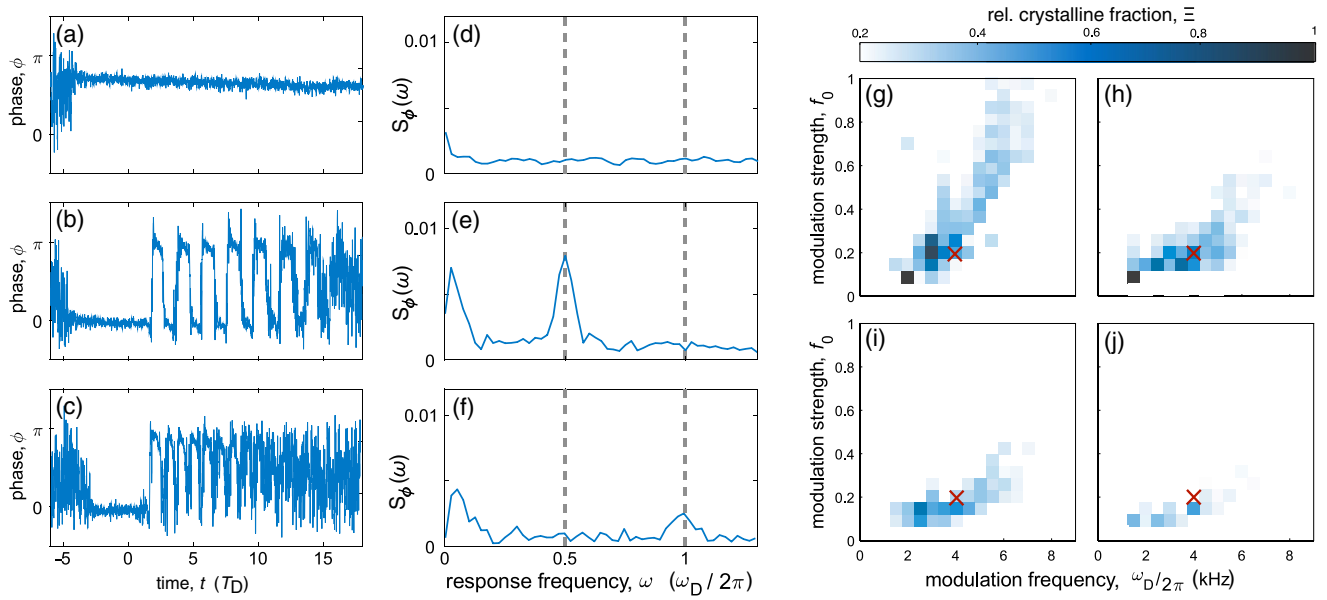

FIG. 2. Dynamical regimes. Dynamics of the relative phase ϕ for (a) $f_0 = 0.05$, (b) $f_0 = 0.25$, and (c) $f_0 = 0.95$ with fixed $\omega_D = 2\pi \times 4$ kHz. (d)–(f) Corresponding Fourier spectra of the dynamics in (a)–(c). As the modulation strength is increased, the system transforms from a DW to a DTC phase. Strong modulation leads to heating and chaotic behavior. (g)–(j) Dynamical phase diagram showing the relative crystalline fraction Ξ as a function of the modulation frequency ω_D and strength f_0 for (g) clean modulation, (h) weak noise strength $n = 9.6$, (i) intermediate noise strength $n = 15.9$, and (j) large noise strength $n = 22.3$. The diagram is constructed by dividing the parameter space into 18×18 plaquettes and within each averaging over multiple experimental runs (at least four realizations). Red crosses in (g)–(j) mark the modulation parameters used in Figs. 3(a)–(d). Increasingly large noise strengths shrink the area in the phase diagram where a stable DTC phase prevails.

contrast to the coherent switching observed in the DTC phase, the chaotic phase is characterized by intermittent dynamics of the relative phase, whereby the system appears to get stuck in one type of checkerboard pattern for two or more consecutive driving cycles [see Fig. 2(c)].

Next, we test the robustness of the DTC against variations of the system parameters and temporal perturbations. To this end, we calculate the relative crystalline fraction Ξ [6,7], defined by means of the amplitude of the subharmonic peak in the normalized Fourier spectrum $S_\phi(\omega)$ of the relative phase ϕ rescaled by its maximum, i.e., $\Xi = S_\phi(\omega_D/2)/S_{\max,\phi}$, where $S_{\max,\phi}$ is the maximum crystalline fraction measured in the parameter space spanned by $f_0 \in [0, 1]$ and $\omega_D \in 2\pi \times [0, 9]$ kHz. Figure 2(g) displays the relative crystalline fraction for varying modulation parameters ω_D and f_0. We observe large relative crystalline fractions $\Xi > 0.2$ for modulation frequencies $\omega_D \in 2\pi \times [2, 8]$ kHz signaling a robust DTC order for a wide range of modulation parameters. Note that the overall shape of the relative crystalline fraction in Fig. 2(g) resembles the stability island of the DTC obtained from numerical simulations using a simple mean-field model (see Ref. [31], Fig. 3).

To explore the robustness of the DTC against temporal perturbations, we introduce a disorder in time by superimposing Gaussian white noise onto the signal of the pump strength. The noise strength is measured by $n \equiv \sum_{\omega=0}^{2\pi\times 50\ \mathrm{kHz}} |\mathcal{E}_{\mathrm{noisy}}(\omega)| / \sum_{\omega=0}^{2\pi\times 50\ \mathrm{kHz}} |\mathcal{E}_{\mathrm{clean}}(\omega)|$, where $\mathcal{E}_{\mathrm{noisy}}$ ($\mathcal{E}_{\mathrm{clean}}$) is the Fourier spectrum of the pump in the presence (absence) of white noise. Figures 2(h)–(j) show how the relative crystalline fraction changes with increasing noise strength. The area with clear DTC response, i.e., a large relative crystalline fraction, shrinks as the noise strength increases. Nevertheless, we still find a sizable region, where a DTC phase exists, for relatively large noise strength [Fig. 2(j)]. For a fixed set of modulation parameters marked by the red crosses in Figs. 2(g)–(j), typical single-shot results for varying noise strengths are depicted in Figs. 3(a)–(d). Note that even for a strongly distorted pump signal, as in Figs. 3(c) and 3(d), the system still switches multiple times between the two sublattices before the intracavity photons disappear. The relative crystalline fraction at fixed modulation parameters decreases with increasing noise strength, as shown in Fig. 3(e). The small offset for large noise strength $n > 25$ is due to the background noise in the Fourier spectrum [see Fig. 2(f)]. Our experimental findings suggest that the DTC in the modulated atom-cavity system is robust against fluctuations not only from the nonunitary dynamics of the dissipative cavity but also from temporal disorder added via driving.

Finally, we address the decay of the time-translation symmetry breaking response in the DTC phase, for example, seen in Fig. 3(a). The experimental lifetimes of time crystal implementations are generally finite due to a

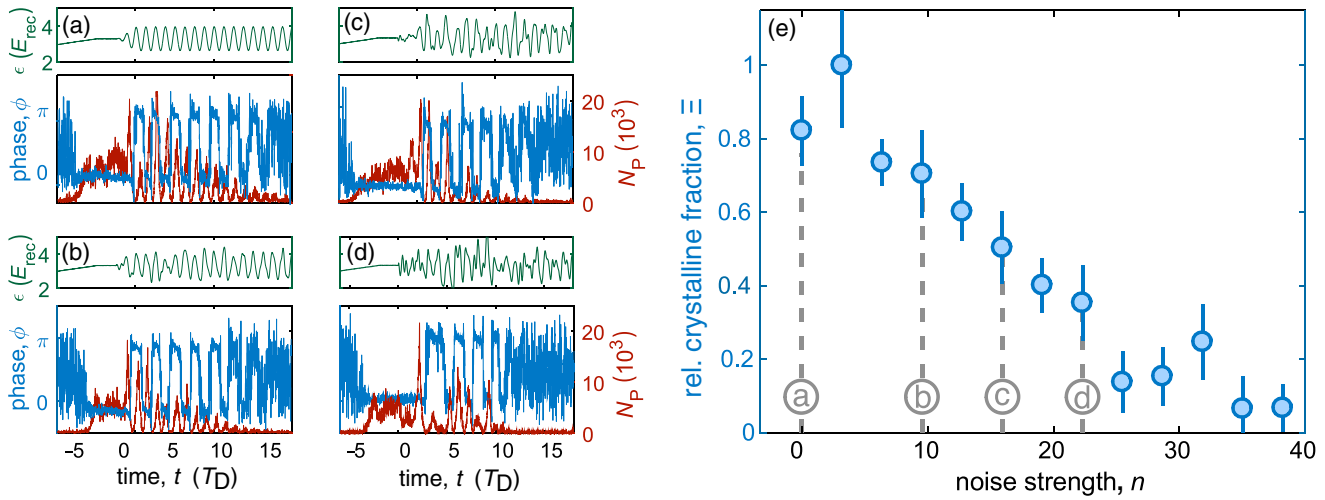

FIG. 3. Robustness of subharmonic response. (a)–(d) Single-shot experimental runs for the noise strengths applied in Figs. 2(g)–(j) and for values of ω_D and f_0 according to the red crosses in these figures. Top panels: single-shot protocols for the pump strength. Bottom panel: corresponding time evolution of the relative phase ϕ (blue trace) and intracavity photon number N_P (red trace). (e) Dependence of the relative crystalline fraction Ξ on the noise strength averaged over 7 experimental runs with $f_0 = 0.2$ and $\omega_D = 2\pi \times 4$ kHz. The gray dashed lines mark the noise strengths used in (a)–(d).

combination of technical limitations and undesired relaxation dynamics [5–7,16,17]. In our experiment, the main cause for the decay of time-crystal dynamics can be attributed to two factors: (i) short-range collisional interaction and (ii) atom losses. In the case of the open Dicke model, the all-to-all coupling between the atoms makes it amenable to a mean-field description. In this theoretical limit, the mean-field solvability of the Dicke model provides the Dicke DTC with the necessary long-range spatiotemporal order and robustness such that it can persists to infinitely long times[19,20]. However, when mean-field breaking terms are present, the DTC may become unstable, leading to a decay of the symmetry breaking response [20]. In the atom-cavity system, the short-range interaction between the atoms competes with the collective coupling, induced by the cavity photons, and breaks the mean-field solvability of the model. To investigate the damping effects of short-range interaction and atom loss, we employ the truncated Wigner approximation (TWA). The transversely pumped atom-cavity system is thereby modeled by considering only the degrees of freedom along the pump (y direction) and the cavity (z direction) axes (see Ref. [31]). The short-range interaction is quantified in terms of the mean-field collisional interaction energy $E_a = (U_a/N_a) \times \int dydz|\psi_0(y,z)|^4$, where U_a denotes the effective two-dimensional interaction strength (see Ref. [31]), N_a is the number of atoms and $\psi_0(y,z)$ is the wave function of the homogeneous BEC. We also include in our model a phenomenological atom loss channel described by $dN_a/dt = -2\gamma N_a$. We simulate the dynamics of the intracavity photon number $N_P = \langle \hat{a}^\dagger \hat{a} \rangle$, where $\hat{a}$ ($\hat{a}^\dagger$) is the bosonic operator that annihilates (creates) a photon in the single-mode cavity. To characterize temporal long-range order, we calculate the two-point temporal correlation function $C(t) = \mathrm{Re}[\langle a^\dagger(t)a(t_0)\rangle]/\langle a^\dagger(t_0)a(t_0)\rangle$ at $t_0 = 0$, the time before the modulation is switched on.

The resulting evolution of $N_P(t)$ and $C(t)$ is studied in Fig. 4 for different values of E_a. First, we consider the dynamics in the absence of atom loss. For weak interaction strength $E_a = 0.08E_{\mathrm{rec}}$, $N_P(t)$ and $C(t)$ in the green traces of Fig. 4 are practically indistinguishable from the findings for $E_a = 0$ in the blue traces. However, stronger short-range interactions with $E_a = 0.30E_{\mathrm{rec}}$ lead to a metastable DTC, where the period-doubling oscillations in $C(t)$ decay after a few cycles, as seen in the red trace in Fig. 4(b). This translates to irregular dynamics of the corresponding intracavity photon number $N_P(t)$ [red trace in Fig. 4(a)] in the long-time regime. Introducing an atom loss channel with $\gamma = 40\ \mathrm{s}^{-1}$, which models the observed atom decay rate in the experiment, yields exponentially decaying behavior as shown in the black traces in Fig. 4. This behavior closely resembles the characteristic exponential decay of N_P in our experiment, such that the cavity is almost empty for $t/T_D > 15$ [see Figs. 3(a)–(d)]. Atom loss leads to a trivial suppression of the atom-cavity coupling and hence of intracavity photons. When the number of intracavity photons falls below the detection level, the relative phase ϕ becomes ill-defined leading to the fast and irregular oscillations of ϕ seen in Figs. 3(a)–(d) for late times. Since we are operating close to the phase boundary between the DW and the normal phase the system is very sensitive to atom loss, which primarily limits the DTC lifetime in the experiment.

Our observations confirm the realization of a dissipative time crystal in an atom-cavity system with the defining feature of period-doubling dynamics. This quintessential

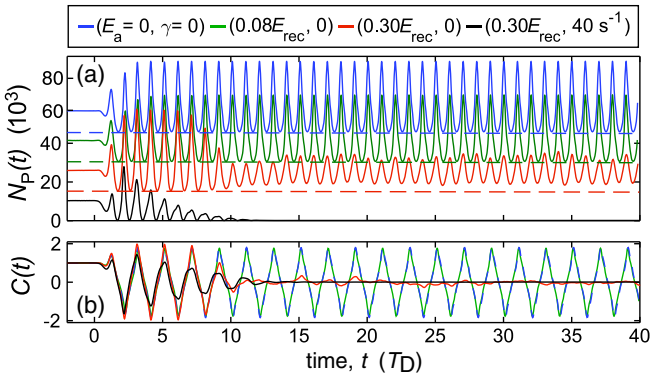

FIG. 4. Short-range interaction and atom loss. Numerical results from TWA for the dynamics of (a) the intracavity photon number N_P and (b) the nonequal time correlation C of the photons for different values of the collisional interaction energy E_a and the atom loss rate γ. To increase the quality of the presentation, the black, red, green, and blue traces in a are plotted with different offsets $0, 15, 30, 45 \times 10^3$, respectively. The modulation parameters are $\omega_D = 2\pi \times 4$ kHz and $f_0 = 0.2$.

DTC is robust against changes of the system parameters and temporal perturbations added to the drive, thereby fulfilling the robustness property of time crystals. Numerical results based on a simplified semiclassical model imply that short-range interaction and atom loss limits the lifetime of the DTC phase.

This work is funded by the Deutsche Forschungsgemeinschaft (DFG, German Research Foundation) SFB-925 Project No. 170620586 and the Cluster of Excellence Advanced Imaging of Matter (EXC 2056), Project No. 390715994.

Note added in the proof.—During submission of this work, a subsequent example of dissipative time crystal was reported in an all-optical system [39].

*Corresponding author.
hkessler@physnet.uni-hamburg.de

[1] F. Wilczek, Quantum Time Crystals, Phys. Rev. Lett. **109**, 160401 (2012).
[2] A. Shapere and F. Wilczek, Classical Time Crystals, Phys. Rev. Lett. **109**, 160402 (2012).
[3] P. Bruno, Impossibility of Spontaneously Rotating Time Crystals: A No-Go Theorem, Phys. Rev. Lett. **111**, 070402 (2013).
[4] H. Watanabe and M. Oshikawa, Absence of Quantum Time Crystals, Phys. Rev. Lett. **114**, 251603 (2015).
[5] J. Zhang, P. W. Hess, A. Kyprianidis, P. Becker, A. Lee, J. Smith, G. Pagano, I. D. Potirniche, A. C. Potter, A. Vishwanath, N. Y. Yao, and C. Monroe, Observation of a discrete time crystal, Nature (London) **543**, 217 (2017).
[6] S. Choi, J. Choi, R. Landig, G. Kucsko, H. Zhou, J. Isoya, F. Jelezko, S. Onoda, H. Sumiya, V. Khemani, C. Von Keyserlingk, N. Y. Yao, E. Demler, and M. D. Lukin, Observation of discrete time-crystalline order in a disordered dipolar many-body system, Nature (London) **543**, 221 (2017).
[7] J. Rovny, R. L. Blum, and S. E. Barrett, Observation of Discrete-Time-Crystal Signatures in an Ordered Dipolar Many-Body System, Phys. Rev. Lett. **120**, 180603 (2018).
[8] K. Sacha and J. Zakrzewski, Time crystals: A review, Rep. Prog. Phys. **81**, 016401 (2018).
[9] D. V. Else, C. Monroe, C. Nayak, and N. Y. Yao, Discrete time crystals, Annu. Rev. Condens. Matter Phys. **11**, 467 (2020).
[10] J. O'Sullivan, O. Lunt, Ch. W. Zollitsch, M. L. W. T., J. J. L. Morton, and A. Pal, Signatures of discrete time crystalline order in dissipative spin ensembles, New J. Phys. **22**, 085001 (2020).
[11] A. Lazarides, S. Roy, F. Piazza, and R. Moessner, Time crystallinity in dissipative Floquet systems, Phys. Rev. Research **2**, 022002 (2020).
[12] K. Sacha, Modeling spontaneous breaking of time-translation symmetry, Phys. Rev. A **91**, 033617 (2015).
[13] D. V. Else, B. Bauer, and C. Nayak, Floquet Time Crystals, Phys. Rev. Lett. **117**, 090402 (2016).
[14] N. Y. Yao, A. C. Potter, I.-D. Potirniche, and A. Vishwanath, Discrete Time Crystals: Rigidity, Criticality, and Realizations, Phys. Rev. Lett. **118**, 030401 (2017).
[15] V. Khemani, A. Lazarides, R. Moessner, and S. L. Sondhi, Phase Structure of Driven Quantum Systems, Phys. Rev. Lett. **116**, 250401 (2016).
[16] S. Autti, V. B. Eltsov, and G. E. Volovik, Observation of a Time Quasicrystal and Its Transition to a Superfluid Time Crystal, Phys. Rev. Lett. **120**, 215301 (2018).
[17] J. Smits, L. Liao, H. T. C. Stoof, and P. van der Straten, Observation of a Space-Time Crystal in a Superfluid Quantum Gas, Phys. Rev. Lett. **121**, 185301 (2018).
[18] R. Chitra and O. Zilberberg, Dynamical many-body phases of the parametrically driven, dissipative Dicke model, Phys. Rev. A **92**, 023815 (2015).
[19] Z. Gong, R. Hamazaki, and M. Ueda, Discrete Time-Crystalline Order in Cavity and Circuit QED Systems, Phys. Rev. Lett. **120**, 040404 (2018).
[20] B. Zhu, J. Marino, N. Y. Yao, M. D. Lukin, and E. A. Demler, Dicke time crystals in driven-dissipative quantum many-body systems, New J. Phys. **21**, 073028 (2019).
[21] B. Buča, J. Tindall, and D. Jaksch, Non-stationary coherent quantum many-body dynamics through dissipation, Nat. Commun. **10**, 1730 (2019).
[22] N. Y. Yao, C. Nayak, L. Balents, and M. P. Zaletel, Classical discrete time crystals, Nat. Phys. **16**, 438 (2020).
[23] H. Ritsch, P. Domokos, F. Brennecke, and T. Esslinger, Cold atoms in cavity-generated dynamical optical potentials, Rev. Mod. Phys. **85**, 553 (2013).
[24] J. Klinder, H. Keßler, C. Georges, J. Vargas, and A. Hemmerich, Bose-Einstein condensates in an optical cavity with sub-recoil bandwidth, Appl. Phys. B **122**, 299 (2016).
[25] K. Baumann, C. Guerlin, F. Brennecke, and T. Esslinger, Dicke quantum phase transition with a superfluid gas in an optical cavity, Nature (London) **464**, 1301 (2010).
[26] J. Klinder, H. Keßler, M. Wolke, L. Mathey, and A. Hemmerich, Dynamical phase transition in the open

Dicke model, Proc. Natl. Acad. Sci. U.S.A. **112**, 3290 (2015).
[27] J. G. Cosme, C. Georges, A. Hemmerich, and L. Mathey, Dynamical Control of Order in a Cavity-BEC System, Phys. Rev. Lett. **121**, 153001 (2018).
[28] C. Georges, J. G. Cosme, L. Mathey, and A. Hemmerich, Light-Induced Coherence in an Atom-Cavity System, Phys. Rev. Lett. **121**, 220405 (2018).
[29] P. Molignini, L. Papariello, A. U. J. Lode, and R. Chitra, Superlattice switching from parametric instabilities in a driven-dissipative Bose-Einstein condensate in a cavity, Phys. Rev. A **98**, 053620 (2018).
[30] J. G. Cosme, J. Skulte, and L. Mathey, Time crystals in a shaken atom-cavity system, Phys. Rev. A **100**, 053615 (2019).
[31] See Supplemental Material at http://link.aps.org/supplemental/10.1103/PhysRevLett.127.043602 for details on the experimental setup, the $\mathbb{Z}_2$ symmetry breaking of the DW phase, and the theoretical model, which includes Refs. [32–36].
[32] D. Nagy, G. Szirmai, and P. Domokos, Self-organization of a Bose-Einstein condensate in an optical cavity, Eur. Phys. J. D **48**, 127 (2008).
[33] A. Polkovnikov, Phase space representation of quantum dynamics, Ann. Phys. (Amsterdam) **325**, 1790 (2010).
[34] P. B. Blakie, A. S. Bradley, M. J. Davis, R. J. Ballagh, and C. W. Gardiner, Dynamics and statistical mechanics of ultracold Bose gases using c-field techniques, Adv. Phys. **57**, 363 (2008).
[35] I. Carusotto and C. Ciuti, Quantum fluids of light, Rev. Mod. Phys. **85**, 299 (2013).
[36] H. Keßler, J. G. Cosme, C. Georges, L. Mathey, and A. Hemmerich, From a continuous to a discrete time crystal in a dissipative atom-cavity system, New J. Phys. **22**, 085002 (2020).
[37] K. Baumann, R. Mottl, F. Brennecke, and T. Esslinger, Exploring Symmetry Breaking at the Dicke Quantum Phase Transition, Phys. Rev. Lett. **107**, 140402 (2011).
[38] J. M. Pino, R. J. Wild, P. Makotyn, D. S. Jin, and E. A. Cornell, Photon counting for Bragg spectroscopy of quantum gases, Phys. Rev. A **83**, 033615 (2011).
[39] H. Taheri, A. B. Matsko, L. Maleki, and K. Sacha, All-optical dissipative discrete time crystals, arXiv:2012.07927.